J Neurophysiol 97: 423–435, 2007.
First published September 27, 2006; doi:10.1152/jn.00547.2006.

Sleep-Related Spike Bursts in HVC Are Driven by the Nucleus Interface of the Nidopallium

Richard H. R. Hahnloser[1] and Michale S. Fee[2]

[1]*Institute of Neuroinformatics, Universität Zürich/Eidgenössische Technische Hochschule Zürich, Zurich, Switzerland; and*
[2]*Department of Brain and Cognitive Sciences and McGovern Institute for Brain Research, Massachusetts Institute of Technology, Cambridge, Massachusetts*

Submitted 22 May 2006; accepted in final form 23 August 2006

Hahnloser, Richard H. R. and Michale S. Fee. Sleep-related spike bursts in HVC are driven by the nucleus interface of the nidopallium. *J Neurophysiol* 97: 423–435, 2007. First published September 27, 2006; doi:10.1152/jn.00547.2006. The function and the origin of replay of motor activity during sleep are currently unknown. Spontaneous activity patterns in the nucleus robustus of the arcopallium (RA) and in HVC (high vocal center) of the sleeping songbird resemble premotor patterns in these areas observed during singing. We test the hypothesis that the nucleus interface of the nidopallium (NIf) has an important role for initiating and shaping these sleep-related activity patterns. In head-fixed, sleeping zebra finches we find that injections of the $GABA_A$-agonist muscimol into NIf lead to transient abolishment of premotor-like bursting activity in HVC neurons. Using antidromic activation of NIf neurons by electrical stimulation in HVC, we are able to distinguish a class of HVC-projecting NIf neurons from a second class of NIf neurons. Paired extracellular recordings in NIf and HVC show that NIf neurons provide a strong bursting drive to HVC. In contrast to HVC neurons, whose bursting activity waxes and wanes in burst epochs, individual NIf projection neurons are nearly continuously bursting and tend to burst only once on the timescale of song syllables. Two types of HVC projection neurons—premotor and striatal projecting—respond differently to the NIf drive, in agreement with notions of HVC relaying premotor signals to RA and an anticipatory copy thereof to areas of a basal ganglia pathway.

INTRODUCTION

Studies of motor-related neural activity and the widely observed replay during sleep are of a broad interest because they relate to the natural mechanisms for encoding and consolidation of memories (Fenn et al. 2003; Nadasdy et al. 1999; Palchykova et al. 2006; Walker and Stickgold 2006). Premotor activity in the songbird nucleus robustus of the arcopallium (RA) is correlated with song vocalizations on a temporal scale in the submillisecond range (Chi and Margoliash 2001; Leonardo and Fee 2005; Yu and Margoliash 1996). RA neuron activity has also been recorded during sleep, where it strongly resembles song-related activity (Dave and Margoliash 2000; Dave et al. 1998). Song and sleep-related spike patterns are believed to be generated by common neural mechanisms because during both singing and sleep, RA spike patterns are driven by sparse sequences in HVC (high vocal center) projection neurons (Hahnloser et al. 2002, 2006). Given that HVC projection neurons are of such importance to RA activity in the singing and sleeping states, we speculate that projection neurons upstream of HVC maybe of similar importance to the generation of sparse HVC sequences. Here we are interested in elucidating the feedforward drive provided to HVC during sleep from the nucleus interface of the nidopallium (NIf).

HVC receives input predominantly from the thalamic nucleus uveaformis (Uva) in the thalamus, the medial magnocellular nucleus of the anterior nidopallium (MMAN), and NIf (Fortune and Margoliash 1995; Nottebohm et al. 1982; Rosen and Mooney 2006; Vates et al. 1996). NIf is embedded in the auditory field L complex and is believed to be important for auditory–motor interactions in the song-control system. Lesions of NIf have been found to abolish selectivity in HVC neurons to acoustic playback of the bird's own song (BOS) (Cardin et al. 2005; Coleman and Mooney 2004; Janata and Margoliash 1999). Similarly, spontaneous activity in HVC of anesthetized birds is strongly reduced after reversible or irreversible NIf lesions (Cardin et al. 2005; Coleman and Mooney 2004).

We are interested in elucidating the sleep-related activity patterns of NIf neurons projecting to HVC (NIf_{HVC} neurons). These NIf neurons were previously identified in anesthetized birds and found to be more densely firing during BOS playback than HVC projection neurons (Coleman and Mooney 2004). Our goal is to identify potential differences in the manner in which these NIf neurons drive activity patterns in downstream areas in the premotor and the anterior forebrain pathways (Okuhata and Saito 1987) involved in song production and song learning (Bottjer et al. 1984; Doupe 1993; Doupe et al. 2004; Scharff and Nottebohm 1991; Sohrabji et al. 1990). To characterize the relationship of sleep-related activity patterns in higher premotor brain areas, we study coherency functions from paired recordings of NIf_{HVC} neurons and HVC projection neurons and, further, study the effects of reversible pharmacological inactivation on sleep-related spike trains. Our study reveals new insights into the dynamics of sleep-related activity patterns. Parts of this presentation were previously published in abstract form (Fee et al. 2002).

METHODS

Our experiments were performed in head-fixed zebra finches, a preparation that permits us to perform paired extracellular recordings from identified neurons and pharmacological manipulations. General methods and procedures for the experimental setup of head-fixed,

Address for reprint requests and other correspondence: R.H.R. Hahnloser, Institute of Neuroinformatics, UZH/ETHZ, Winterthurerstrasse 190, 8057 Zurich, Switzerland (E-mail: rich@ini.phys.ethz.ch).

The costs of publication of this article were defrayed in part by the payment of page charges. The article must therefore be hereby marked "*advertisement*" in accordance with 18 U.S.C. Section 1734 solely to indicate this fact.

sleeping birds and spike train data analysis were described previously (Hahnloser et al. 2006).

Subjects

Zebra finches (*Taeniopygia guttata*) were obtained from commercial suppliers (Old Bridge, NJ and Animal Diffusion, Villarimboud, Switzerland). Animals were maintained on a day–night reversed 12-h light cycle to assist in obtaining sleep during daytime experimental sessions. Data were taken from a total of 36 adult zebra finches (>90 days).

Surgery

Surgery began approximately at the onset of the night cycle. Birds were anesthetized with 1–3% isoflurane in oxygen. A small hole (about 200 μm) was made in the dura over each area and the uncovered brain was protected with 2% low-melting agarose (Sigma). Bipolar stimulation electrodes (Teflon-insulated 50-μm-diameter stainless steel wire spaced 0.5 mm apart) were inserted into HVC and RA or Area X and secured to the scull with dental acrylic. Wound margins were treated with lidocaine gel. The animal was placed in a small foam restraint and subsequently moved to the recording apparatus without further anesthesia. In some of the experiments, to promote sleep, the bird was given a single dose (1–10 μg) of melatonin (Sigma) right after surgery, injected subcutaneously in phosphate-buffered saline.

Electrophysiology

ANTIDROMIC ACTIVATION. Bipolar stimulation electrodes in HVC were used for antidromic identification of NIf neuron type and RA (or Area X) stimulation electrodes were used for identification of HVC neuron type (Fig. 1*A*). Electrical stimulation was produced using an isolated stimulation unit (AMPI) with intensities varying from 50 to 500 μA. For most experiments, single monophasic current pulses of 0.2-ms duration were used as stimuli. Single or paired single-unit recordings were made in HVC and NIf. High signal-to-noise (>10:1) recordings were made using sharp glass microelectrodes (5–15 MΩ, borosilicate, 1.0 mm OD, 0.7 mm ID) pulled on a vertical electrode puller (Model 730, Kopf Instruments) and filled with 2 M NaCl. Signals were amplified using a Neurodata IR285 (Cygnus Instruments) or Axoclamp-2B (Axon Instruments) intracellular amplifiers. Custom electronics were used for additional amplification (gain of 100) and filtering (300-Hz high-pass five-pole Bessel filter, 10-kHz low-pass constant delay filter). Extracellular signals were digitized to 16-bits precision at a sampling rate of 20 kHz and stored in blocks of 200 s on a Pentium-based PC running custom LabVIEW software (National Instruments).

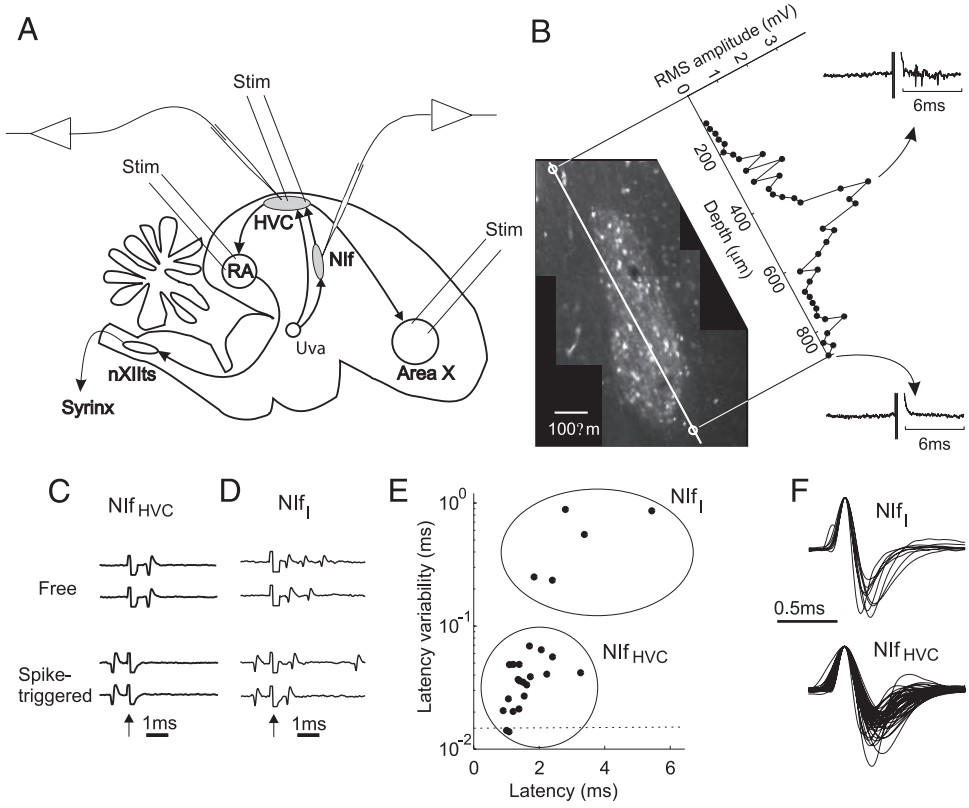

FIG. 1. Nucleus interface of the nidopallium (NIf) and NIf neuron identification. *A*: schematics of the song-control system and the experimental setup. NIf receives input from the thalamic nucleus uveaformis (Uva) and projects to HVC (high vocal center). HVC projects to the robust nucleus of the arcopallium (RA), which in turn innervates vocal motor neurons in the hypoglossal nucleus (nXIIts). NIf neuron type was identified by antidromic stimulation in HVC and HVC neuron type by antidromic stimulation in RA or Area X. *B*: NIf extent, as assessed by the region of increased response to stimulation agrees with histological identification. NIf was retrogradely labeled by fluorescent dextran injection in HVC. Two white circles close to the extremes of the white line mark electrolytic lesions used as reference points along the electrode track. Shown in the tilted axes is the root-mean-square (RMS) extracellular voltage amplitude in the interval 1–7 ms after stimulation onset. RMS amplitude is high ($\gtrsim$1 mV) when the electrode is inside NIf and low otherwise. *C*: electrical stimulation in HVC elicits spike responses in NIf_{HVC} neurons at a single precise time lag (*top*). Stimulating 0.5 ms after a spontaneous spike in a NIf_{HVC} neuron leads to response failure (*bottom*). *D*: antidromic responses in NIf_I neurons have larger latency variability (*top*) and do not fail when HVC is stimulated right after a spontaneous spike (*bottom*). The arrows in *C* and *D* mark the stimulation artifacts. *E*: a plot of spike latency vs. latency variability allows for segregation of NIf_{HVC} neurons from NIf_I neurons based on a latency-variability threshold of 0.1 ms. *F*: spike waveforms of NIf_{HVC} neurons (*top*) and of NIf_I neurons (*bottom*) are very similar.

NIF LOCALIZATION. For the NIf identification experiment in Fig. 1*B*, we first pressure-injected 200 nl of 10% fluorescent dextran in phosphate-buffered saline into right HVC. The purpose of this tracer injection was to fluorescently label NIf neurons. Two days later, under anesthesia, we penetrated NIf from a posterior angle with a 1- to 3-MΩ platinum tungsten electrode. Every 20 μm between 2- and 3-mm penetration depth, we recorded the responses to 30 HVC stimulations at 1-s intervals (about 200-μA amplitude). After assessing the extent of NIf by observing the stimulation responses on an oscilloscope, we made two electrolytic lesions above and below NIf, 900 μm apart. Lesions were made by injecting a constant current of 15 μA for about 12 s. These lesions were later identified in histological sections to precisely locate the electrode track within sagittal slices of the brain. Stimulation response shown in Fig. 1*B* was quantified by the root-mean-squared (RMS) voltage amplitude in the 1- to 7-ms interval after stimulation onset (averaged over the 30 stimulations per site).

NIF NEURON IDENTIFICATION. NIf neurons were found and isolated using ongoing 1-Hz stimulation in HVC to elicit spike responses. Once a cell was isolated, stimulation threshold current was measured and stimulus intensity was set between 10 and 50% above threshold to produce a reliable response. Continuous analog records were acquired for 60 stimuli at 1-s intervals. The response latency of an antidromic spike is defined as the interval between stimulus onset and the first evoked spike. Latency variability is defined as the SD of response latency. We estimate that the contribution to the latency variability arising from our fixed sampling rate of 20 kHz is <16 μs (dashed line in Fig. 1*E*). Because neurons in neighboring field L may also project to HVC (Fortune and Margoliash 1995), we tried to avoid recording from field-L neurons by recording only from those NIf regions with very dense multiunit response (hash) to stimulation, shown to correlate well with NIf extent (Fig. 1*B*). Furthermore, we observed that field L neurons projecting to HVC (L_{HVC} neurons) had longer response latencies to HVC stimulation than did NIf_{HVC} neurons. Also, L_{HVC} neurons showed strong phasic responses to brief sound clicks, whereas NIf_{HVC} neurons did not. For the NIf neurons classified as interneurons, we were similarly conservative and applied this classification only to neurons found at penetration depths within the electrophysiologically identified borders of NIf.

REVERSIBLE LESIONS IN NIF. The effect of lidocaine and muscimol injections in NIf on sleep-burst rate in HVC interneurons was examined by microinjection of lidocaine or muscimol in 2% phosphate-buffered saline during single-unit recordings of HVC_I neurons. Injections were made from pulled glass pipettes (50-μm tip size) using a pressure-injection system (Pico Spritzer). Injected volumes were 10–100 nl. Control injections were made in NIf with phosphate-buffered saline. Typically, injection pipettes were placed in the center of NIf after an electrophysiological recording session during which the extent of NIf was well characterized by multiple electrode penetrations. To measure the effect of the injection, we counted the number of bursts in the HVC_I neuron in the minute before and after the injection. Statistical significance of burst-rate differences before and after the injection was assessed using the Mann–Whitney *U* test ($P < 0.001$). In one case the bird woke up right after the injection (by observation of eye opening). Because the burst rate in HVC neurons is known to be highly state dependent (Hahnloser et al. 2006), data from this trial were discarded.

HISTOLOGY. After each experiment, the animal was killed by intramuscular injection of 20% urethane or nembutal. For the NIf identification experiment, birds were transcardially perfused with 4% paraformaldehyde (PFA) in 25 mM $NaPO_4$ buffer. The brain was removed for histological examination of Nissl-stained (or unstained) slices to verify the location of stimulating and recording electrodes and drug injection sites. All experiments were carried out in accord with protocols approved by the local IACUC and the Veterinary Amt of the Canton of Zurich, Switzerland.

Spike train analysis

All spike train analysis procedures were implemented with custom-made Matlab (The MathWorks, Natick, MA) scripts.

INSTANTANEOUS FIRING RATE. One way of representing the activity at time t of a neuron is by the instantaneous firing rate $R(t)$, a continuous function defined by the inverse of the interspike interval (ISI) surrounding time t.

BURST RATE. We identified a group of at least two spikes as a burst if the instantaneous firing rate continuously exceeded 100 Hz. The burst rate is defined as the number of events per unit time in which the instantaneous firing rate crosses the 100-Hz barrier from below.

ISI PROBABILITY DENSITY FUNCTION (PDF). For each neuron A we computed the ISI pdf $h_A(\tau)$ as a basic characterization of its spike train (τ stands for the ISI). First we computed the ISI histogram with bin centers τ_i, chosen on a logarithmic scale ($i = 1, \ldots, 100$). The ISI pdf $h_A(\tau_i)$ is simply a normalized ISI histogram satisfying $\Sigma_i\, h_A(\tau_i) = 1$.

AUTOCOVARIANCE FUNCTION. The autocovariance function $C_{AA}(t)$ of a spike train $\rho_A(t)$ (modeled as a sum of delta functions) is a measure of spike density fluctuations. It is computed as

$$C_{AA}(t) = \frac{1}{T - |t|} \int_0^T \rho_A(s + t)\rho_A(s)\mathrm{d}s - \overline{\rho_A}^2 \qquad (1)$$

where $\overline{\rho_A}$ is the mean firing rate of neuron A and T is the duration of the recording (the denominator $T - |t|$ results in an unbiased estimation of autocovariance at large times $t \ll T$). The first term on the right side of *Eq. 1* is known as the *autocorrelation function*. By subtracting the term $\overline{\rho_A}^2$ in *Eq. 1*, the asymptotic value of the autocovariance function is zero. For better visibility, we plotted autocovariance functions on a logarithmic timescale t_i in Fig. 3, *C* and *D* by integration between adjacent points, i.e., the discrete function $C_{AA}(i) = \int_{t_i}^{t_{i+1}} C_{AA}(t)\mathrm{d}t$ is plotted.

To assess the complexity of spike trains, we probed them for renewal dynamics, i.e., we tested whether ISIs were generated by random sampling from the ISI pdf $h_A(\tau)$. Renewal spike trains have no memory because each ISI is a random variable that is independent of the previous ISI. To perform this test, we computed renewal autocovariance functions $C^R_{AA}(t)$ derived from the ISI pdfs under renewal assumptions (here superscript R stands for renewal) and compared these functions to the measured autocovariance functions. For a derivation of $C^R_{AA}(t)$ see, e.g., Gerstner and Kistler (2002). Any deviation of $C_{AA}(t)$ from $C^R_{AA}(t)$ is indicative of a memory in the spike train, causing ISIs to be conditional on previous ISIs. A deviation at time t_i is significant if $C^R_{AA}(i)$ differs from $C_{AA}(i)$ by >3SE of $C_{AA}(i)$ (the SE was computed by jackknifing; see METHODS on the coherency analysis).

We also tested whether autocovariance functions differed from renewal functions on the population level. Average autocovariance functions $\langle C_{AA}(t)\rangle_A$ and $\langle C^R_{AA}(t)\rangle_A$ for the two NIf neuron types are shown by the full and dashed lines in Fig. 3, *C* and *D*. At each time t_i we tested whether the autocovariance and renewal functions at that time had identical medians using the Wilcoxon rank-sum test ($P < 0.01$). Time intervals where deviations were significant are indicated by thick horizontal bars in Fig. 3, *C* and *D*.

COHERENCY ANALYSIS. We quantified correlations between spike trains in simultaneously recorded cells by the coherency function $\gamma_{AB}(t)$, which is similar to the cross-covariance function, but includes an additional normalization by the autocovariance functions of the two spike trains. This normalization serves to discount for correlations

arising from bursting tendencies of neurons (Kimpo et al. 2003; Thomson and Chave 1991). In the frequency domain ω, the coherency function $\gamma_{AB}(\omega)$ is computed by normalizing the cross-covariance function $C_{AB}(\omega)$ between neurons A and B by the square roots of the autocovariance functions

$$\gamma_{AB}(\omega) = \frac{C_{AB}(\omega)}{\sqrt{C_{AA}(\omega)C_{BB}(\omega)}} \quad (2)$$

We determined the coherency in the time domain $\gamma_{AB}(t)$ by inverse Fourier transformation of $\gamma_{AB}(\omega)$. As in our previous study (Hahnloser et al. 2006), we smoothed the coherency function $\gamma_{AB}(t)$ by convolution with a Gaussian windowing function of 4-ms SD. Finally, the smoothed coherency functions were downsampled to 1-ms temporal resolution by summing over coherencies in 1-ms bins. Our findings do not critically depend on the parameter values for smoothing and downsampling.

To depict the typical coherency function between neuron types, we plotted the average coherency function $\langle \gamma_{AB}(t) \rangle_{AB}$ (Figs. 6, *C* and *E* and 7, *B* and *D*).

SIGNIFICANCE. The significance threshold for the coherency function of a particular neuron pair was assessed by jackknifing the data in 10-s data windows and computing the jackknife variance (Thomson and Chave 1991)

$$\sigma_J^2(t) = \frac{N-1}{N} \sum_{i=1}^{N} [\gamma_{AB}^i(t) - \bar{\gamma}_{AB}(t)]^2$$

where N represents the number of data windows (depending on the duration of the recording), $\gamma_{AB}^i(t)$ is the coherency function of the jackknifed data with the ith window missing, and $\bar{\gamma}_{AB}(t) = \langle \gamma_{AB}^i(t) \rangle_i$ is the average coherency function of the jackknifed data.

We set the significance threshold of measured coherencies to $3\sigma_J(t)$, shown by dashed lines in Figs. 6 and 7. This threshold corresponds to a roughly 99% confidence for the significance test. Whenever the coherency function exceeded the significance threshold, a peak emerged. The distributions of peak amplitudes versus peak latencies are shown in the summary plots beneath the average coherency functions in Figs. 6, *C* and *E* and 7, *B* and *E*.

We also analyzed coherency functions on a population level, to see whether they had some characteristic shape. For all neuron pairs of given types, the average coherency function was compared with the average significance threshold shown by dashed lines in Figs. 6, *C* and *E* and 7, *B* and *D*. Characteristic peaks in average coherency functions were found by testing whether differences between the coherency functions and the significance thresholds had zero median using the Mann–Whitney signed-rank test ($P < 0.01$). Time intervals where the median coherency function was significantly larger than the median renewal function are indicated by thick horizontal bars in Figs. 6*C* and 7*D*.

RESULTS

We set out to characterize the role of NIf input for generating and shaping sleep-related spontaneous activity in identified HVC neurons. Because different types of NIf neurons were not previously classified, and their firing properties and correlations with identified HVC neurons during sleep are unknown, we *1*) distinguished NIf_{HVC} neurons from other NIf neuron types using antidromic activation by electrical stimulation in HVC, *2*) analyzed spike train statistics of identified NIf neurons, and *3*) assessed spike train correlations and coherencies of identified NIf and HVC neurons. Furthermore, to characterize the properties of population activity in NIf and assess its relevance for shaping spike trains in HVC, we *4*) pharmacologically blocked NIf activity while recording spike trains from identified HVC neurons. All our recordings and manipulations were performed in the sleeping, head-fixed bird (see METHODS). A schematic of the zebra finch brain showing NIf and HVC and the location of stimulation and recording electrodes is shown in Fig. 1*A*.

NIf localization

NIf is surrounded by auditory areas of the field-L complex (L1, L2, and L3). Because neurons in field L1 and L3 have projection targets in the shelf of HVC, one could imagine confounding them with NIf neurons when searching for antidromic responses to HVC stimulation. However, there are cytoarchitectural and morphological differences between NIf and areas of the field-L complex. Cytoarchitectural studies revealed increased cell density in NIf compared to that in L1 and L3, and morphological studies revealed differences in predominant Golgi cell types found in NIf and field L (Fortune and Margoliash 1992, 1995). Based on these studies we expected to find increased density of extracellular responses to HVC stimulation when placing the recording electrode inside NIf.

By quantifying the multiunit response density (stimulation hash) by the root-mean-squared (RMS) voltage trace in a small time interval after HVC stimulation, we indeed found a robust increase in RMS voltage when the recording electrode was positioned within NIf (Fig. 1*B*). In this experiment, we verified the passage of the electrode track through NIf by examining histological sections of the brain in which NIf was retrogradely labeled by fluorescent indicator (see METHODS). In the following experiments, we used the clearly visible increase in stimulation hash at short stimulus latencies as an operational assessment of NIf extent. All single-unit recordings were performed at penetration depths within this antidromically characterized region.

Classification of NIf neurons

We identified two distinct NIf response patterns to HVC stimulation (Fig. 1, *C* and *D*). Putative HVC-projecting NIf neurons responded to low-intensity stimulation (50–500 μA) in HVC with a single spike. Near-threshold stimulation produced latencies to the first spike between 0.9 and 3.2 ms (average 1.6 $\pm$ 0.6 ms, $n = 20$) with small latency variability in the range 14–69 μs (37 $\pm$ 16 μs, $n = 20$, Fig. 1*E*). Putative NIf interneurons responded to low-intensity stimulation in HVC, with an increasing number of spikes for increasing stimulus intensity. Near-threshold stimulation produced latencies to the first spike ranging from 1.8 to 5.4 ms (mean 3.2 $\pm$ 1.4 ms, $n = 5$) and a large latency variability in the range 236–887 μs (559 $\pm$ 317 μs, $n = 5$, Fig. 1*E*). On the basis of these results, we infer that the neurons with small latency variability were HVC-projecting (NIf_{HVC}) neurons. For simplicity, we refer to the neurons with large latency variability as NIf interneurons (NIf_I neurons), although we cannot rule out that these neurons project outside of NIf. In agreement with this classification, in all cases tested ($n = 20$), we found that neurons with latency variability <100 μs (putative NIf_{HVC} neurons) exhibited spike collisions when stimulated immediately after a spontaneous spike (Fig. 1*C*, *bottom*). Neurons with latency variabilities >100 μs (putative NIf_I neurons), on the other hand, did not exhibit collisions (Fig. 1*D*, *bottom*). The

vast majority of neurons isolated within the borders of NIf, as defined by the presence of antidromic hash, had small-latency variability and had firing patterns as described below for NIf_{HVC} neurons. Long-latency variability neurons were rarely found and all of these had firing patterns similar to those described below for NIf_I neurons. In the subsequent experiments, we identified each recorded NIf cell by its antidromic stimulation response, distinguishing NIf_I neurons from NIf_{HVC} neurons by their differences in spike latency variability.

The spike widths, measured at 25% of the peak amplitude, were smaller for NIf_I neurons (0.16 ± 0.02 ms, range 0.13–0.19 ms, $n = 9$) than they were for NIf_{HVC} neurons (0.20 ± 0.04 ms, range 0.13–0.32 ms, $n = 51$, Fig. 1*F*). However, based on the considerable overlap between spike width distributions, we were unable to classify neuron type based on spike width or even spike waveform (using principal component analysis).

In many simultaneous recordings in NIf and HVC, we also identified HVC neuron type by RA stimulation. In the course of these experiments, we found two neurons in NIf (in two birds) that projected both to HVC and to RA, as judged by the spike collision test. However, we were not able to determine whether these neurons formed monosynaptic connections with both HVC and RA neurons or whether the axonal pathways of these HVC-projecting neurons simply passed in close proximity to RA, but without targeting RA neurons. Note that RA has not been identified as a projection target of NIf neurons in the literature.

Spike train properties of two NIf neuron types

During sleep, a large fraction of spikes in both NIf neuron types fell into high-frequency bursts (Fig. 2, *A* and *B*). Nevertheless, NIf_{HVC} and NIf_I neurons differed considerably in their spontaneous firing patterns during sleep. For example, the average firing rate of NIf_{HVC} neurons was 5.4 Hz, whereas that of NIf_I neurons exceeded 27 Hz. NIf_{HVC} neurons fired fewer bursts per second and exhibited larger average instantaneous firing rates during bursts than did NIf_I neurons (Wilcoxon rank-sum test, $n = 117$ NIf_{HVC} neurons and $n = 13$ NIf_I neurons, $P < 0.01$). Average firing rates, firing rates during bursts, burst rates, burst widths, number of spikes per burst, and the fraction of total spikes that are part of bursts are summarized in Table 1.

In our previous recordings we found that firing rates in HVC and RA neurons waxed and waned, altering between a state of high firing lasting 1–2 s and a state of low firing also lasting several seconds (Hahnloser et al. 2006). We previously identified a suitable timescale to measure these firing-rate fluctuations to be 3 s. When analyzed in similar 3-s windows, we did not find similarly large fluctuations of firing rates in NIf neurons. Average firing rates of NIf_{HVC} neurons were distributed in the range from 0 to ≤22 Hz (filled circles in Fig. 2*C*).

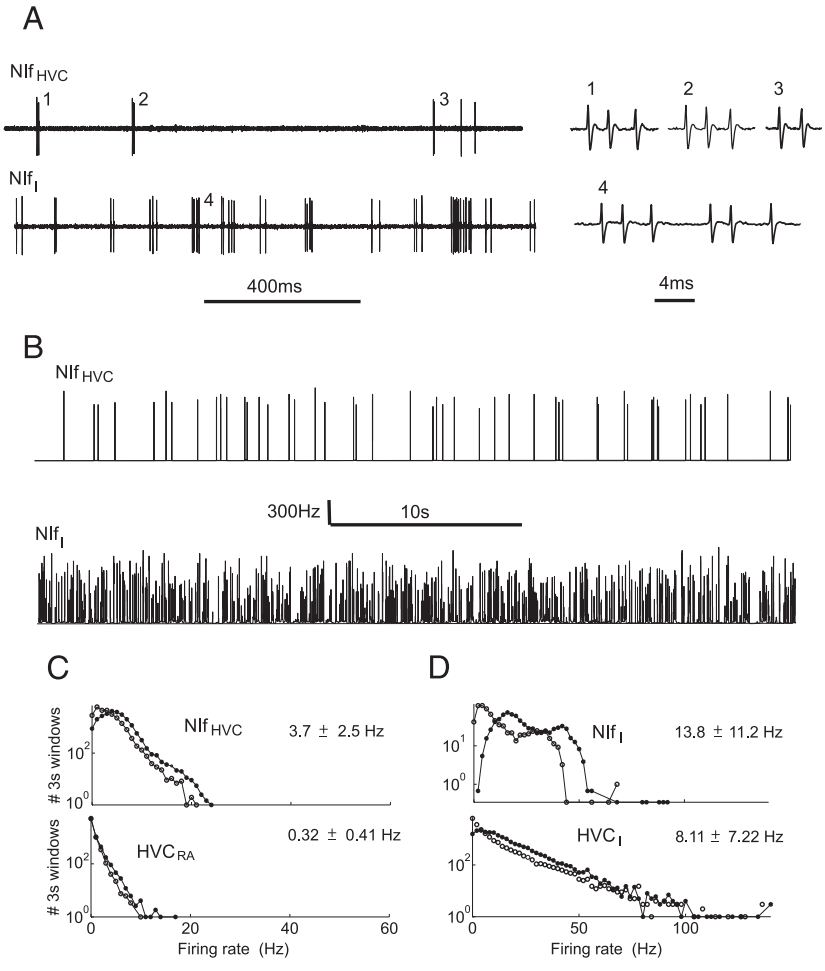

FIG. 2. NIf neuron spike trains during sleep. *A*: extracellular records of a NIf_{HVC} neuron (*top*) and a NIf_I neuron (*bottom*). Burst events labeled on the *left* are redrawn on a smaller timescale on the *right*. *B*: instantaneous firing rate (IFR) functions of a NIf_{HVC} neuron (*top*) and a NIf_I neuron (*bottom*). *C*: firing-rate distribution of NIf_{HVC} neurons and (*D*) NIf_I neurons in 3-s windows. Filled symbols are average firing rates in regular spike trains; open symbols are from burst spike trains with single spikes removed. Numbers shown on the *right* are average firing rates ± SDs for the burst spike trains, computed after removing single spikes.

TABLE 1. *Firing statistics for two NIf neuron types*

Neuron Type	Firing Rate, s^{-1}	Burst Firing Rate, s^{-1}	Burst Rate, s^{-1}	Burst Width, ms	Spikes per Burst	Spikes in Bursts, %
NIf_{HVC} ($n = 117$)	5.4 ± 3.3	461 ± 139	1.4 ± 0.9	4.4 ± 1.7	2.7 ± 0.5	70 ± 20
Awake NIf_{HVC} ($n = 5$)	5.0 ± 1.9	550 ± 173	1.2 ± 0.6	3.7 ± 1.2	2.5 ± 0.3	58 ± 19
NIf_I ($n = 13$)	27.8 ± 9.6	321 ± 87	4.9 ± 2.9	7.5 ± 1.7	3.0 ± 0.9	53 ± 24

Values are means ± SD.

This range of firing rates is comparable to that of HVC_X neurons, an HVC neuron type of average firing rate less than a third that of NIf_{HVC} neurons. NIf_I neurons rarely displayed firing rates <5 or >50 Hz (Fig. 2*D*). In comparison, HVC_I neurons, despite having half the average firing rate, achieved about twice the range of NIf_I firing rates. In Fig. 2, *C* and *D*, we also show firing-rate distributions of NIf neurons in burst spike trains (spike trains for which all single spikes not part of a burst have been removed for the analysis), verifying that on a coarse timescale, small firing-rate fluctuations also applied to bursts.

This lack of extensive firing-rate fluctuations in NIf motivated us to measure spike train statistics in NIf_{HVC} neurons also in awake birds, as judged by their open eyes after touching their tails ($n = 3$ birds). In data from 3-min recording sessions, we found that firing rates and burst rates of NIf_{HVC} neurons in the awake state were not statistically different from the firing rates measured during sleep (Wilcoxon rank-sum test, $n = 5$ NIf_{HVC} neurons, $P < 0.01$; Table 1). Note that in our previous sleep studies in HVC and RA, we never observed bursts in awake birds in any neuron type.

ISI and autocovariance functions

We decided to further study NIf spike trains and the biophysical mechanisms responsible for their generation by examining ISI probability density functions (pdfs), and autocovariance functions. These functions are computed and analyzed in the following.

The average ISI pdf of each NIf neuron type is bimodal, with a common first peak corresponding to the ISIs during bursts and a second peak roughly corresponding to the interburst interval (Fig. 3, *A* and *B*). The average ISI pdf of NIf_{HVC} neurons is reminiscent of that of HVC projection neurons because these neurons also emit virtually no spikes at an ISI of about 10 ms (Hahnloser et al. 2006). Similarly, the average ISI pdf of NIf_I neurons is reminiscent of that of HVC_I neurons.

In HVC projection neurons there is evidence of intrinsic (not synaptically driven) bursting as judged by the stereotypy of recorded sleep bursts (Hahnloser et al. 2002), whereas in HVC interneurons and RA neurons, there is no such evidence (Dave and Margoliash 2000). We investigated the burst stereotypy of NIf neurons by computing autocovariance functions. In 83 of 117 NIf_{HVC} neurons, we found an oscillatory behavior of autocovariance functions on a very short timescale, with an example shown in the *inset* of Fig. 3*C*. This oscillatory behavior is a consequence of stereotyped burst patterns and suggests a cellular rather than a network mechanism for burst generation in NIf_{HVC} neurons. Only one of 13 NIf_I neurons showed an oscillatory autocovariance function, thus providing weaker evidence for intrinsic bursting mechanisms in NIf_I neurons (a

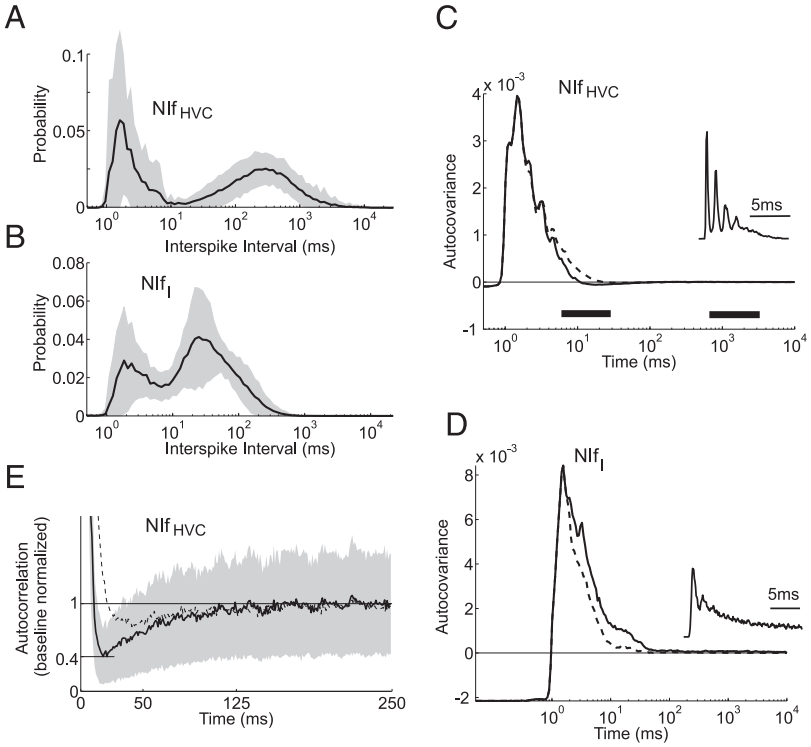

FIG. 3. Interspike interval (ISI) probability density functions (pdfs) and autocorrelation functions. *A*: average ISI pdf of NIf_{HVC} neurons, with the shaded area representing ± SD. There are few ISIs of about 10 ms and few ISIs >1 s. *B*: average ISI pdf of NIf_I neurons shows virtually no ISIs >400 ms. *C*: average autocovariance function of NIf_{HVC} neurons plotted on a logarithmic timescale. Delta-function peak at *time 0* has been suppressed. Dashed line is the average renewal autocovariance function derived from the respective ISI pdfs. In the interval close to 10 ms, the autocovariance function is smaller than the renewal function and, in the interval around 1 s, it is larger (as indicated by the 2 thick horizontal bars below the autocovariance function). *Inset*: autocovariance function of the NIf_{HVC} neuron from Fig. 2*B*, reflecting stereotyped bursting behavior by the oscillatory shape. *D*: average autocovariance function of NIf_I neurons is larger than the renewal function, but this difference is not significant. *Inset*: autocovariance function of the NIf_I neuron from Fig. 2*B*. *E*: average autocorrelation function of NIf_{HVC} neurons plotted on a linear timescale, clearly displaying the soft refractory period of about 125 ms during which the spiking probability is reduced to at most 40% of baseline.

typical nonoscillatory autocovariance function is shown in the *inset* of Fig. 3*D*).

The simplest generative process of a spike train with a given ISI pdf is the renewal process, according to which each ISI is drawn randomly and independently of other ISIs from a fixed ISI pdf. By exploring whether NIf neuron spike trains are compatible with a renewal process for their generation, we derived from their ISI pdfs expected autocovariance functions under renewal assumptions (see METHODS). By comparison with these renewal (autocovariance) functions, we found further evidence for intrinsic bursting tendencies in NIf_{HVC} neurons. Of the 109 NIf_{HVC} neurons tested, 57 exhibited autocovariance functions that were smaller than the equivalent renewal functions somewhere in the time interval 3–45 ms (jackknife, $P < 0.01$). Other than these cases, no significant differences with renewal statistics were observed. This absence of long sequences of short ISIs suggests a limitation of NIf_{HVC} neurons to produce long bursts. In this respect, NIf_{HVC} neurons are similar to HVC projection neurons, in which a similar trend was seen.

A different behavior was seen in NIf_I neurons. Of the 13 NIf_I neurons tested, 10 exhibited autocovariance functions compatible with renewal assumptions and three exhibited autocovariance functions larger than renewal functions somewhere in the interval 3–31 ms. This behavior of NIf_I neurons is reminiscent of RA and HVC_I neurons, in which bursts were also found to be longer than expected by renewal statistics.

Given these diverse behaviors of individual NIf neurons, we also tested their compatibility with renewal statistics on the population level. We found that the median autocovariance function of NIf_{HVC} neurons was smaller than the median renewal function in the time interval 6–30 ms (Kruskal–Wallis test, $P < 0.01$). However, the median autocovariance function of NIf_I neurons was not significantly different from the median renewal function (Kruskal–Wallis test, $P < 0.01$, Fig. 3*D*). In conclusion, renewal tests in two NIf neuron types reveal differences between their burst-generation mechanisms. Some form of depressive dynamics seems to shorten NIf_{HVC} neuron bursts, whereas no such mechanism appears to apply to NIf_I neurons.

NIf_{HVC} neurons display a firing decrement in their autocorrelation function. In the range of about 10–100 ms, the average autocorrelation function of NIf_{HVC} neurons clearly dips below its asymptotic value (Fig. 3*E*). In this time range, NIf_{HVC} neurons exhibit a reduced spike probability down to 40% of baseline. We have not observed such a firing decrement in any other neuron type in NIf, HVC, RA, or lateral magnocellular nucleus of the anterior nidopallium (LMAN); it may represent a soft refractory period unique to NIf_{HVC} neurons.

Reversible lesions in NIf

To determine the role of NIf_{HVC} population activity for the generation of sleep bursts in HVC, we examined the effect of reversible inactivation of NIf while recording activity in single HVC_I neurons (Fig. 4). When we injected the sodium-channel blocker lidocaine into NIf, the spontaneous bursting of HVC_I neurons immediately stopped (Fig. 4*A*) and recovered after about 3–4 min (Fig. 4*A*, *bottom*). The HVC_I neuron burst rate in the 60-s interval after the injection was significantly smaller than that in the 60-s interval preceding the injection (Mann–Whitney *U* test, $P < 0.01$, $n = 3/3$ birds, three injections per bird, Fig. 4*C*). Saline injections did not lead to a significant change in HVC_I neuron burst rates (Mann–Whitney *U* test, $P < 0.01$, $n = 3/3$ birds, three injections per bird). We realized that a caveat of our lidocaine injections was that they might

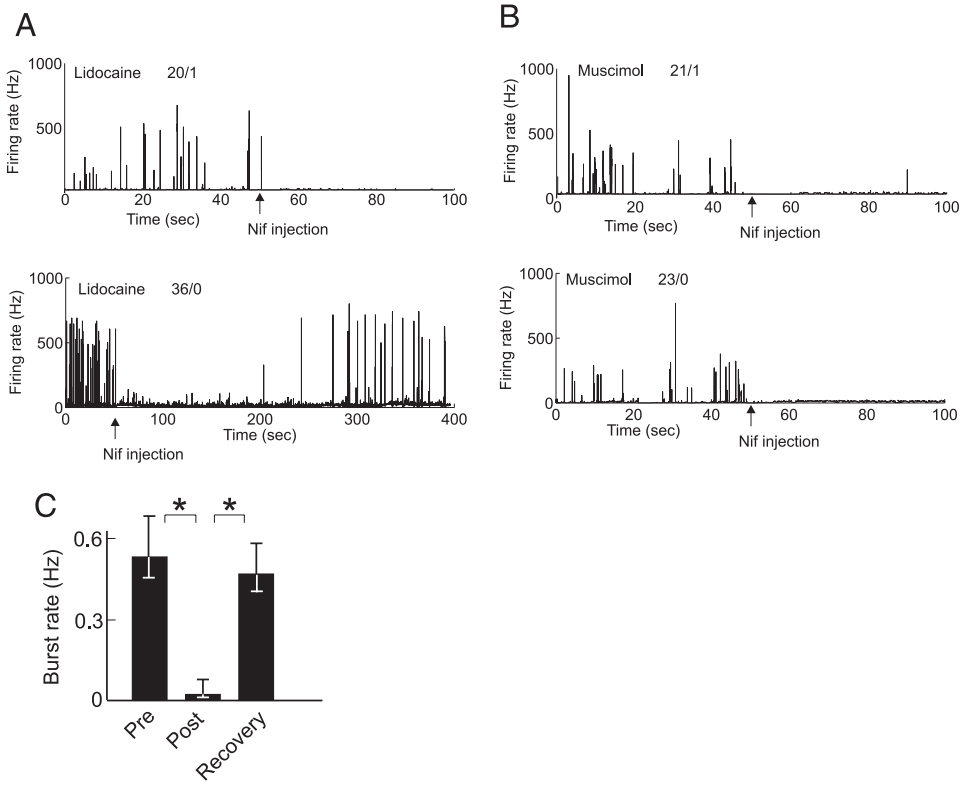

FIG. 4. Effect of lidocaine and muscimol injections into NIf on sleep burst rate in HVC_I neurons. Numbers separated by a backslash indicate the number of bursts measured in the 50-s interval before the injection and after the injection. *A*: lidocaine injections into NIf immediately disrupt bursting in HVC_I neurons, as can be seen from the instantaneous firing rates of 2 HVC_I neurons (*top* and *bottom*). Bursting recovers within 3–4 min (*bottom*). *B*: muscimol injections into NIf have a similar effect of reducing burst rate in HVC_I neurons, but no recovery is observed on this timescale. *C*: median postinjection burst rates of HVC_I neurons were significantly lower than median preinjection rates for both muscimol and lidocaine injections. Burst rates recovered after 5 min of lidocaine injections to values similar to preinjection rates. Error bars delimit the upper and lower quartiles and the asterisks denote significant differences (Mann–Whitney *U* test, $P < 0.01$).

also have affected fibers of passage from Uva to HVC. To restrict the effect of injections to neural dendrites and somata in the NIf region, we also injected the γ-aminobutyric acid type A ($GABA_A$) agonist muscimol into NIf. Similarly as for the lidocaine injections, we observed an immediate and significant reduction in HVC_I neuron burst rate in the minute after the muscimol injection (Mann–Whitney U test, $P < 0.01$, $n = 3/3$ birds, three injections per bird, $P < 0.01$, Fig. 4*B*). Recovery of burst rates was not observed within more than 20 min after muscimol injections. Despite these reduced burst rates, we found that HVC_I neurons kept spiking after NIf inactivation (see Fig. 4, *A* and *B*), suggesting that lidocaine and muscimol did not leak into HVC. Furthermore, the average firing rate of HVC_I neurons in the 50 s after lidocaine or muscimol injections into NIf was 10.2 ± 5.4 Hz and so was smaller than the typical firing of HVC_I neurons during sleep: 15 ± 9.0 Hz (Hahnloser et al. 2006), but was not significantly different from average firing rates of these neurons measured in the awake bird: 7.2 ± 7.0 Hz (Hahnloser et al. 2006). These results suggest that NIf provides essential input to HVC that is necessary to transform the regular spiking of HVC_I neurons in the awake state into bursting in the sleeping state. The reduced firing and bursting of HVC_I neurons after NIf inactivation agrees with previous inactivation and norepinephrine injection experiments in the anesthetized bird (Cardin and Schmidt 2004b; Coleman and Mooney 2004).

Paired recordings in identified HVC and NIf neurons

To directly compare firing properties of NIf neurons with those of HVC neurons, we performed paired recordings in these areas. NIf neuron type was identified by antidromic stimulation in HVC and HVC neuron type was identified by antidromic stimulation in either RA or Area X.

From our single-neuron recordings we know that NIf_{HVC} neurons have a weak, but significant tendency to form burst epochs (in Fig. 3*C*, in the time interval 0.75–3.4 s the median autocovariance function is larger than the median renewal function, Kruskal–Wallis test, $P < 0.01$). However, as to be expected, in paired recordings of NIf_{HVC} and HVC_I neurons, we observed much stronger burst epochs in HVC_I neurons than in NIf_{HVC} neurons (Fig. 5*A*). To analyze cofluctuations of firing rates in more detail, we computed correlation coefficients of firing rates measured in nonoverlapping 3-s windows. For

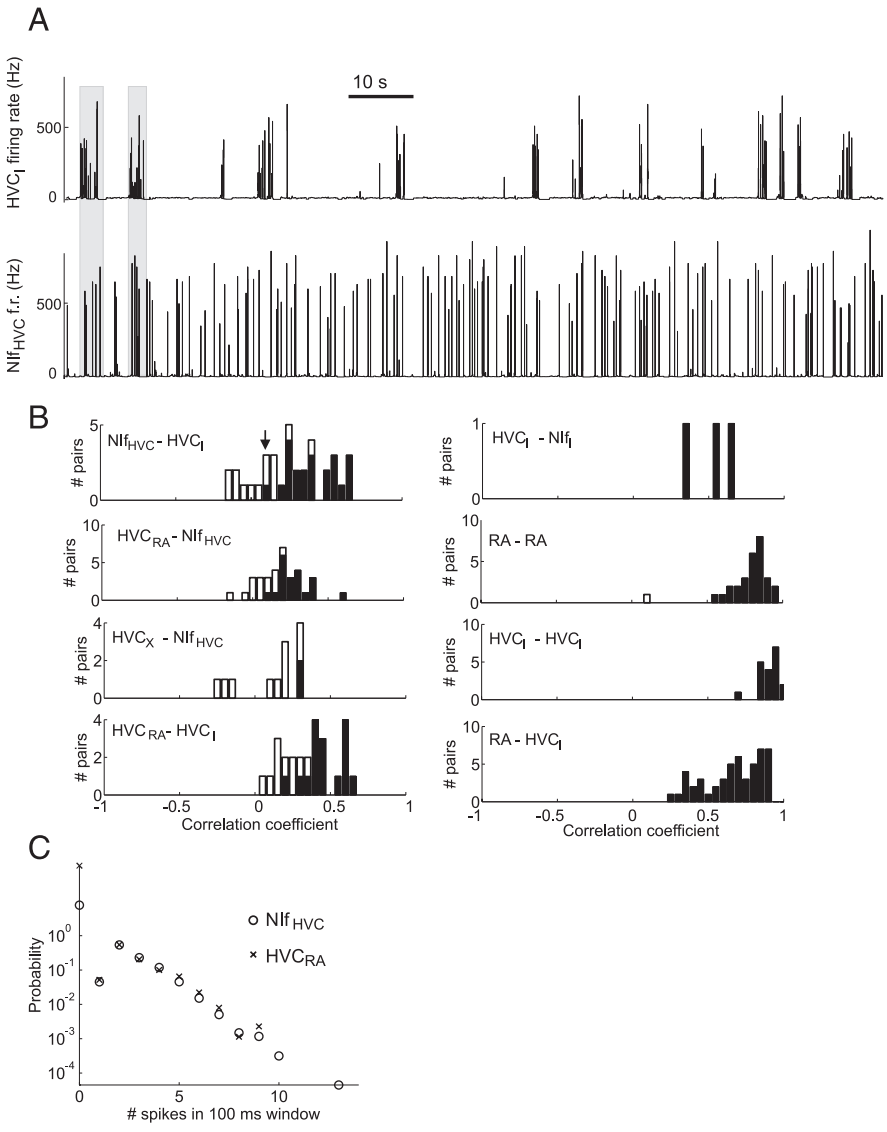

FIG. 5. Burst density variations in NIf_{HVC} and HVC_I neurons are weakly correlated. *A*: instantaneous firing rates in a simultaneously recorded NIf_{HVC}–HVC_I neuron pair. Clustering of HVC_I neuron spikes into burst epochs is only weakly reflected in the NIf_{HVC} neuron (2 burst epochs in the HVC_I neuron that seem to be coincident with increased bursting in the NIf_{HVC} neuron are marked by shaded areas). *B*: correlation coefficients of firing rates measured in 3-s windows of simultaneously recorded neuron pairs. Black bars represent significantly correlated pairs ($P < 0.01$). Correlations among neuron pairs involving HVC or NIf projection neurons are often not significant and smaller (*left row*) than correlations among other neuron pairs (*right row*). Arrow indicates the correlation coefficient of the neuron pair in *A*. *C*: by performing the same analysis as in Fig. 2*C*, but on a time window of 100 ms instead of 3 s, we find identical firing-rate distributions in NIf_{HVC} and HVC_{RA} neurons. To produce this subfigure we analyzed burst-train data from 34 simultaneously recorded neuron pairs. As illustration, the "probabilities" of zero spikes in NIf_{HVC} and HVC_{RA} neurons are also shown; these differ dramatically, but are not taken into account for comparing the distributions.

the neuron pair shown in Fig. 5*A*, the correlation coefficient of 0.15 was found to be significant ($P < 0.05$). In fact, most NIf_{HVC}–HVC_I neuron pairs showed significantly correlated firing rates (Fig. 5*B*, *top left*). By incorporating previously recorded data in HVC into our analysis (Hahnloser et al. 2006), we found that NIf_{HVC}–HVC_I firing-rate correlations are comparable to those of HVC_{RA}–HVC_I neurons (Fig. 5*B*, *bottom left*). Similarly, firing rates in most NIf_{HVC}–HVC_{RA} neuron pairs were significantly correlated, and also some NIf_{HVC}–HVC_X neuron pairs showed correlated firing rates. Thus on the level of firing-rate correlations with HVC_I neurons, there is a similarity between NIf and HVC projection neurons, despite their large differences in burst rates.

The firing-rate correlations involving interneurons in NIf and HVC are stronger and more reliable than those involving projection neurons in NIf and HVC. In 99 neuron pairs not involving a projection neuron in either HVC or NIF, we found only one pair that did not exhibit significantly correlated firing rates (Fig. 5*B*, *right*). Average correlation coefficients for all neuron pairs studied are summarized in Table 2.

To further test for similarities between NIf_{HVC} and HVC_{RA} neurons, we compared firing-rate distributions in paired recordings of NIf_{HVC} and HVC_{RA} neurons. Average firing rates in these neurons differed by about one order of magnitude (NIf_{HVC}: 5.4 ± 3.3 Hz vs. HVC_{RA}: 0.6 ± 0.9 Hz, $n = 34$ pairs), as did average burst rates (NIf_{HVC}: 1.4 ± 0.9 Hz vs. HVC_{RA}: 0.13 ± 0.2 Hz, $n = 34$ pairs). However, we found a striking similarity between firing-rate distributions of NIf_{HVC} and HVC_{RA} neurons after discounting for baseline differences in firing rates. That is, we counted the number of spikes fired in 100-ms windows of burst spike trains by taking into account windows where only at least one spike was found (thus discounting for differences in the number of empty windows). In 22 of 34 NIf_{HVC}–HVC_{RA} neuron pairs, we found indistinguishable firing-rate distributions in the two cells [Kolmogorov–Smirnov (K-S) test, $P < 0.01$]. Similarly, the distribution of firing rates of the entire NIf_{HVC} population was identical to the distribution of the HVC_{RA} population (K-S test, $P < 0.01$, Fig. 5*C*). Equality of firing-rate distribution in these different populations was robust and was observed for analysis windows in the range of the soft refractory time of NIf_{HVC} neurons, i.e., from 50 to 150 ms. Firing similarity was less striking for other HVC neuron types. In three of 12 NIf_{HVC}–HVC_X neuron pairs we found equal firing-rate distributions (also not counting empty windows). Moreover, in only three of 37 NIf_{HVC}–HVC_I neuron pairs did we find equality of firing-rate distributions (likewise not counting empty windows). Equality of firing-rate distributions on the population level and in 100-ms windows was observed for NIf_{HVC}–HVC_{RA} cell pairs only.

TABLE 2. *Sleep-related firing-rate correlations and burst ratios in different neuron pairs, measured in nonoverlapping 3-s windows*

Neuron Pair	Number of Correlated Pairs	Correlation Coefficient	Median Burst-Rate Ratio
NIf_{HVC}–HVC_I	22/37, 13 birds	0.42 ± 0.17	1.2
HVC_I–NIf_I	3/3, 3 birds	0.51 ± 0.15	3.2
HVC_{RA}–NIf_{HVC}	19/33, 12 birds	0.28 ± 0.11	19.6
HVC_{RA}–HVC_I	16/26, 6 birds	0.42 ± 0.12	46.8
HVC_X–NIf_{HVC}	2/12, 4 birds	0.29 ± 0.01	—
HVC_I–HVC_I	19/19, 5 birds	0.91 ± 0.06	—
RA–RA	28/29, 3 birds	0.79 ± 0.1	—
RA–HVC_I	50/50, 9 birds	0.66 ± 0.19	3.4

Correlation coefficients (means ± SD) were computed for significantly correlated pairs only. The criterion for significance was $P < 0.05$. The median burst-rate ratios in the last column were computed by the median value of ratios of average firing rates in simultaneously recorded pairs of neurons, single spikes removed. In the denominator for this ratio, we always choose the neuron appearing on the left in the first column. For example, NIf_I neurons fired 3.2 times as many spikes in burst trains as did HVC_I neurons.

To study the relationship between spikes in NIf_{HVC} neurons and HVC projection neurons on a high temporal resolution, we examined raster plots of NIf_{HVC} neuron activity aligned on HVC_{RA} neuron bursts. We quantified the paired recordings by coherency functions, derived from the full spike trains including single spikes. We found that very often the HVC_{RA} neuron bursts were preceded by NIf_{HVC} neuron bursts by just a few milliseconds (Fig. 6, *A* and *B*). For most NIf_{HVC}–HVC_{RA} neuron pairs, we found one significant peak in the coherency function (20/34 pairs exhibited each one significant peak at median time lag of −5 ms, in the range −21 to 1 ms; 14/34 pairs exhibited no significant peak, Fig. 6*C*, *bottom*). The average coherency function between NIf_{HVC} and HVC_{RA} neurons exhibited a peak at −5 ms, well above the average significance threshold (Fig. 6*C*, *top*). The median coherency function was above the median significance threshold in the time interval from −7 to −5 ms (Wilcoxon signed-rank test, $P < 0.01$). Thus NIf_{HVC} neurons on average spike just a few milliseconds before HVC_{RA} neurons do.

We also examined raster plots of NIf_{HVC} activity aligned on HVC_X neuron bursts. In many pairs, as was the case with HVC_{RA} neurons, bursts in HVC_X neurons tended to be preceded by NIf_{HVC} neuron bursts. However, in some cases, bursts in the HVC_X neuron preceded the NIf_{HVC} neuron bursts (Fig. 6*D*). In summary, most NIf_{HVC}–HVC_X neuron pairs exhibited at least one significant coherency peak (8/12 pairs exhibited at least one significant peak at median time lag −2 ms, in the range −8 to 20 ms, Fig. 6*E*). The three main peaks at a positive time lag in Fig. 6*E* are from three different birds and are unlikely to be a sampling artifact. The average coherency function between NIf_{HVC} and HVC_X neurons exhibited two distinct peaks, one peak at −3.5 ms, well above the average significance threshold, and the other at 15 ms, roughly coinciding with the average significance threshold (Fig. 6*E*, *top*). From these data, differences between the two types of HVC projection neurons are apparent. At a positive time lag >5 ms there was no peak in 34 pairs with HVC_{RA} neurons, whereas there were six peaks in 12 pairs with HVC_X neurons. The only HVC_{RA} neuron we found to somewhat reliably burst before the NIf_{HVC} neuron was the one shown in Fig. 6*B*. However, as can be seen, significance of the coherency function at a positive time lag was not achieved.

In paired recordings of NIf_{HVC} neurons with HVC_I neurons we observed frequent bursts in the HVC_I neuron in close proximity to NIf_{HVC} neuron bursts (Fig. 7*A*). In most NIf_{HVC}–HVC_I neuron pairs there was at least one significant peak in the coherency function (32/37 pairs exhibited at least one significant peak with a median time lag of 7 ms, range −24 to 123 ms, Fig. 7*B*, *bottom*). In agreement with the notion that NIf_{HVC} neurons tend to burst before HVC_I neurons, the average coherency function between NIf_{HVC} and HVC_I neurons exhibited a peak at 5 ms, well above the average significance threshold

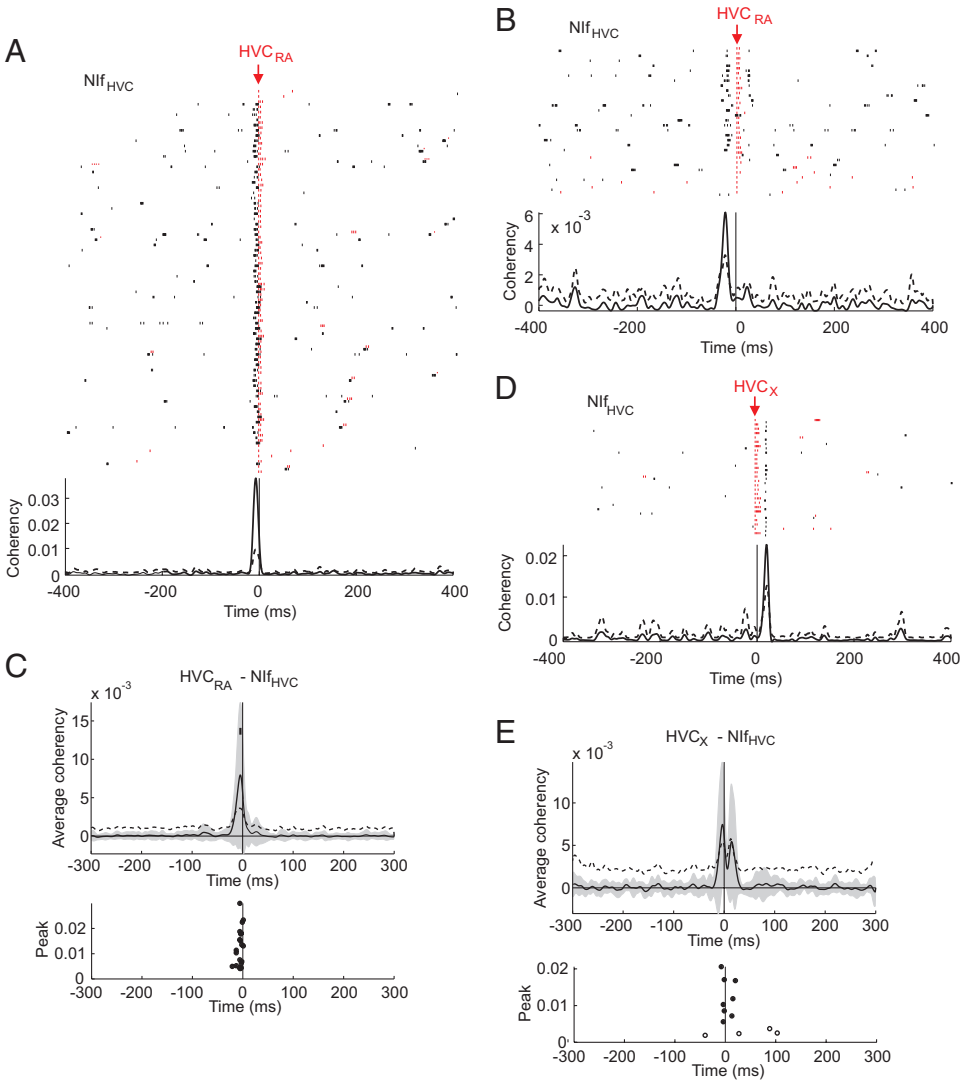

FIG. 6. Paired recordings of NIf neurons and HVC projection neurons. *A*: spike raster plot of simultaneously recorded NIf_{HVC} and HVC_{RA} neuron pair. Spike bursts of the HVC_{RA} neuron (short red lines) are aligned on the first spike at the center of the plot. Corresponding NIf_{HVC} spikes (short black lines) are shown below each HVC_{RA} burst. NIf_{HVC} neuron bursts tend to precede the HVC_{RA} neuron bursts by a few milliseconds. Below the raster plot is the coherency function plotted as a black line, with the significance threshold shown by the dashed line. Full line exceeds the dashed line in a peak at −8 ms, indicating significant coherency. *B*: same analysis for another NIf_{HVC}–HVC_{RA} neuron pair. Again, significant coherency exists at a negative time lag. Few bursts in the NIf_{HVC} neuron that follow the HVC_{RA} neuron bursts are not significant as can be seen in the *bottom*. *C*: summary of all HVC_{RA}–NIf_{HVC} neuron pairs. *Top*: full line shows the average coherency function between all HVC_{RA}–NIf_{HVC} neuron pairs. Shaded area delimits the SD of coherency functions. Dashed line shows the average significance threshold. There is a narrow coherency peak at a negative time lag where the median coherency is larger than the median significance threshold (thick horizontal bar). *Bottom*: all significant coherency peaks from individual neuron pairs. *D*: raster plot of a HVC_X–NIf_{HVC} neuron pair. NIf_{HVC} neuron bursts reliably after the HVC_X neuron (with significant coherency). *E*: summary of HVC_X–NIf_{HVC} neuron pairs. Average coherency function (*top*) exhibits significant peaks at −3.5 and at 15 ms. Peaks of individual coherency functions are found at both positive and negative time lags in the range −40 to 100 ms. Full circles denote the main peaks of individual neuron pairs; open circles denote significant secondary peaks (of smaller coherency value than the main peak).

(Fig. 7*B*, *top*). The median coherency function of NIf_{HVC}–HVC_I pairs was significantly larger than the median significance threshold in the time interval from 2 to 14 ms (Wilcoxon signed-rank test, $P < 0.01$).

We were not able to record from many NIf_I neurons. An example raster plot of a NIf_I neuron, simultaneously recorded with an HVC_{RA} neuron is shown in Fig. 7*C*. There was a highly significant coherency peak as a result of the many NIf_I neuron bursts produced just a few milliseconds before the HVC_{RA} neuron bursts. On the level of a small population, we could verify this tendency (3/3 HVC_{RA}–NIf_I pairs exhibited at least one significant peak with a median time lag of −9 ms).

For the paired recordings of NIf_I neurons with HVC_I neurons we did not produce raster plots because of the high burst densities in both of these neuron types. Coherency plots peaked significantly at a small negative time lag with respect to HVC_I neuron spikes (3/3 significant pairs with median time lag of −4 ms in the range −9 to −2 ms), showing that the NIf_I neurons were strongly coherent with HVC_I neurons (Fig. 7*D*).

In conclusion, the time lags of coherency peaks were in agreement with a causal relationship between NIf neuron spikes and subsequent activity in HVC. Some of our observations suggest interesting mechanisms by which NIf neurons drive bursts in HVC neurons during sleep, discussed in the next section.

DISCUSSION

We found that NIf neurons can reliably be identified in extracellular recordings by antidromic stimulation from HVC. Antidromic response latencies in NIf_{HVC} neurons were very short and narrowly clustered, suggesting that synchronized bursts in NIf could lead to short-latency bursts in HVC with very little temporal jitter. Compared with NIf_{HVC} neurons, NIf_I neurons responded to HVC simulation with much larger latency variability. We observed many distinguishing characteristics of spontaneous activity in these two different NIf neuron types, including mean firing rates, burst rates, and burst-generation mechanisms.

Given the absence of any known projection target of NIf other than HVC, we speculate that the second NIf neuron type belongs to a class of interneurons. One reason for our speculation is based on the high burst rates in NIf_I neurons, analogous to interneurons in RA and HVC (Hahnloser et al. 2006; Leonardo and Fee 2005). With RA and HVC interneurons

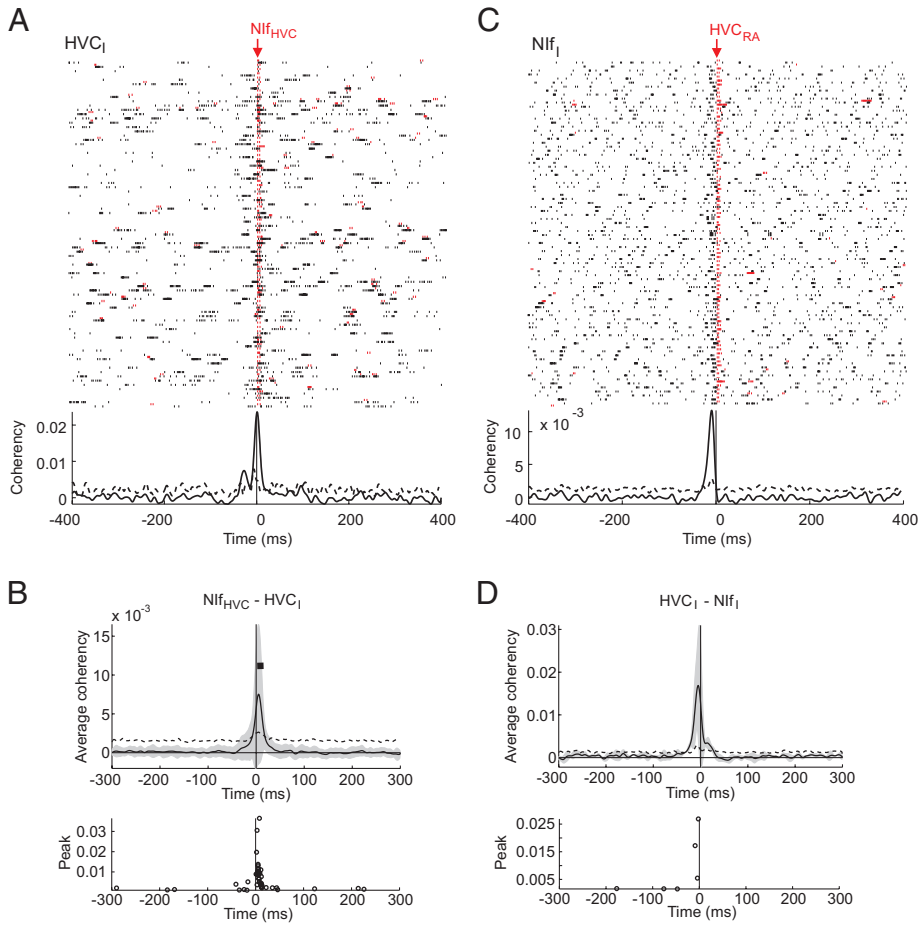

FIG. 7. Raster plots involving HVC_I and NIf_I neurons. *A*: raster plot of HVC_I neuron spikes, time-aligned on NIf_{HVC} neuron bursts. Below, the coherency function peaks 1 ms after NIf_{HVC} neuron spikes. *B*: average coherency function of NIf_{HVC}–HVC_I neurons peaks 1 ms after NIf_{HVC} neuron spikes (*top*). Individual peaks are almost exclusively located at positive time lags of NIf_{HVC} neuron spikes. *C*: raster plot of NIf_I neuron spikes, time-aligned to HVC_{RA} neuron bursts. Coherency function significantly peaks −9 ms before HVC_{RA} neuron spikes (*bottom*). *D*: average coherency function of HVC_I–NIf_I neuron pairs peaks −6 ms before HVC_I neuron spikes (*top*). All 3 neuron pairs exhibit significant coherency peaks at a small negative time lag (*bottom*).

being inhibitory (Rosen and Mooney 2003; Spiro et al. 1999), it may well be that NIf_I neurons are inhibitory as well. This classification is quite plausible, given that our GABA and muscimol injection experiments and previous such experiments (Cardin and Schmidt 2004a; Coleman and Mooney 2004) strongly suggest an abundance of GABA receptors in NIf. However, further experiments will be necessary to determine the neurotransmitter type released by NIf_I neurons.

We suspect the high coherencies between NIf_I and HVC neurons arise from common input from NIf_{HVC} neurons, just as HVC_I neurons are strongly coherent with RA neurons, likely by virtue of common input from HVC_{RA} neurons (Hahnloser et al. 2006). Currently, the only evidence that NIf_I neurons are synaptically driven by NIf_{HVC} neurons is that they respond with short latency to HVC stimulation, shown here to antidromically activate NIf_{HVC} neurons. More paired NIf_I and HVC recordings would help to further clarify the relationship between NIf_I and HVC activity.

We did not find significant differences between firing rates of NIf neurons in the awake and the sleeping states. This finding contrasts with a previous study where arousal of lightly sedated birds led to reduction of spontaneous NIf activity (Cardin and Schmidt 2004a). This apparent disagreement might arise from differences between the sedated state and the sleeping state or might be attributed to effects of residual melatonin in our experiments. In any case, we believe the most interesting phenomenon to be that NIf cells burst in the awake state, a property that has never been observed in either RA or HVC cells.

We speculate that there exists a mechanism that gates the response of HVC to ongoing drive from NIf, much as there is a mechanism that gates the transmission of auditory responses in HVC from NIf (Cardin and Schmidt 2003, 2004b). According to our view, NIf_{HVC} neurons would constantly bombard and occasionally activate HVC projection neurons. Not all of these events would necessarily result in a dense sleep-burst epoch in HVC, to agree with the moderate firing-rate correlations of NIf_{HVC} and HVC projection neurons with HVC_I neurons in Fig. 5. However, on some occasions, a dense sleep-burst epoch would form, activating most HVC neurons. Because we found a weak but nonnegligible tendency of NIf_{HVC} neurons to also form sleep-burst epochs (Figs. 3*C* and 5, *A* and *B*), we speculate that Uva might somehow control the generation of sleep-burst epochs, for example, by coordinating neuromodulatory input (Akutagawa and Konishi 2005). Further influences on HVC excitability might also result from input from the MMAN (Foster and Bottjer 2001; Foster et al. 1997), as well as from direct cholinergic (Shea and Margoliash 2003) or other neuromodulatory input to HVC (Appeltants et al. 2000).

To our surprise, despite large differences between average firing rates in NIf and HVC projection neurons, we also found many similarities on a global and a local level. First, NIf_{HVC} and HVC_{RA} neurons have a similar burst density on the level of the entire population, when considering that burst rates in

NIf_{HVC} neurons were tenfold higher, but their population size is about tenfold smaller. Also, thanks to their soft refractoriness on the timescale of song syllables (about 100 ms), firing-rate distributions of NIf_{HVC} neurons were found to be identical to those of HVC_{RA} neurons (Fig. 5*C*).

A central question pertaining to NIf output is whether NIf activity serves only to initiate a sequence of self-sustained sleep bursts in HVC or whether every single burst in HVC is driven by a particular set of NIf bursts. In the former case, a particular set of strongly synchronized bursts in NIf might serve as the single initialization signal for the HVC bursts. In the latter case, transiently increased burst rates in NIf might lead to repeated excitation of HVC neurons beyond their firing thresholds. Our paired recordings involving NIf_{HVC} neurons can be helpful to tease these two possibilities apart. Our main observation was an interesting difference in the coherencies of NIf_{HVC} neurons with the two types of HVC projection neurons. HVC_{RA} neurons burst reliably just after NIf_{HVC} neurons did, whereas HVC_X neurons burst reliably after *and* before NIf_{HVC} neurons. From the coherencies with HVC_{RA} neurons we would be led to conclude our first hypothesis—that NIf activity serves to initialize HVC sleep-burst sequences—is correct. However, the HVC_X bursts preceding the NIf_{HVC} bursts suggest that, at least on the timescale of a few milliseconds, NIf neurons engage in stereotyped sequential activity. Thus the more complete picture suggested by our data is that there is a first population burst in NIf that activates mainly HVC_X neurons. Then, a second population burst just a few milliseconds later activates HVC_{RA} and HVC_X neurons. Such a scenario can explain why HVC_{RA} bursts are rarely observed to precede NIf_{HVC} bursts, whereas HVC_X neurons are observed to frequently burst before and after NIf_{HVC} neurons. It is interesting to note that, in our previous recordings of HVC neuron pairs (Hahnloser et al. 2006), whereas most HVC_X - HVC_{RA} pairs were not coherent, the single pair we found that showed coherent bursting did so with the HVC_X neuron leading by roughly 20 ms. Coherency differences between the two types of HVC projection neurons might result from two distinct classes of NIf_{HVC} neurons, from HVC-intrinsic mechanisms such as inhibition (Mooney 2000; Solis and Perkel 2005) or from other brain areas such as Uva. For example, Uva projection neurons might directly drive HVC_X neurons and indirectly drive HVC_{RA} neurons by activation of NIf.

We can speculate about the functional role of the observed latency differences between HVC_{RA} and HVC_X neurons. It is clear that signals originating in HVC and arriving in RA take longer if they do so by traveling along the anterior forebrain pathway involving Area X (Okuhata and Saito 1987) than by traveling directly from HVC to RA. Thus the anticipatory firing of HVC_X neurons can partially compensate for signal delays that would normally occur if they fired simultaneously with HVC_{RA} neurons. The signal propagation time from HVC to RA along the anterior forebrain pathway has been estimated to be around 40 ms (Abarbanel et al. 2004; Kimpo et al. 2003; Troyer and Doupe 2000). With our measured time difference of 20 ms (15 + 5 ms) between the second peak in HVC_X coherency functions and the first peak in HVC_{RA} coherency functions, it follows that about half the signal propagation time along the anterior forebrain pathway is compensated for by anticipated departure of HVC_X neuron signals. With an estimated propagation time of 4 ms for HVC_{RA} signals to reach RA (Hahnloser et al. 2006), we conclude that bursts in NIf tend to reach RA by the premotor pathway 16 ms before they reach RA by the anterior forebrain pathway.

What could be the purpose of such a latency adjustment? Some previous models of vocal learning emphasized the importance of differences in propagation delay through the premotor pathway and through the anterior forebrain pathway. In these models HVC_X activity is to be viewed as an efference copy of premotor signals in HVC_{RA} neurons (Abarbanel et al. 2004; Troyer and Doupe 2000). Given the known modulatory role of LMAN for song (Kao et al. 2005; Olveczky et al. 2005; Scharff and Nottebohm 1991), anticipation of HVC signals transmitted along the anterior forebrain pathway could be important to maintain proper registration of premotor signals along the two efferent pathways of HVC.

Given our acute experimental protocol, we were unable to relate individual spike patterns in the sleeping bird to premotor activity during singing. Therefore we analyzed burst events, knowing that bursting in HVC and in RA is a signature of the singing state. Our reversible inactivation experiments provide new insights into the role of NIf for burst generation in HVC (Fig. 4). Given the strong correlations between HVC_I neurons and other HVC neuron types during sleep (Hahnloser et al. 2006), and given the strong reduction of auditory-evoked subthreshold activity in all HVC neuron types after NIf inactivation (Coleman and Mooney 2004), we speculate that NIf drives sleep bursts in all HVC neuron types and, presumably, also in RA. Such a role of NIf during sleep is highly remarkable given that NIf neurons exhibit singing-related activity (Hahnloser and Fee 2003; McCasland 1987), although HVC seems to be able to produce song-related bursts in adult zebra finches with bilateral NIf lesions (Cardin et al. 2005). In combination with the loss of auditory responses in HVC neurons after NIf inactivation (Coleman and Mooney 2004), our results imply a surprising involvement of NIf in conveying song-specific activity, both on a replay and on a sensory level. With the possibility of existence of off-line learning mechanisms during sleep (Deregnaucourt et al. 2005; Margoliash 2001; Nadasdy et al. 1999), we could imagine that auditory hallucination of the BOS originating in NIf is the driving force of such memory consolidation processes.

ACKNOWLEDGMENTS

We thank M. Minkoff and three anonymous reviewers for comments on the manuscript.

GRANTS

These studies were supported by a Swiss National Science Foundation grant and a Forschungskredit of the University of Zurich to R. Hahnloser and National Institute of Mental Health Grant RO1-MH-067105 to M. S. Fee.

REFERENCES

Abarbanel HDI, Gibb L, Mindlin GB, Rabinovich MI, and Talathi S. Spike timing and synaptic plasticity in the premotor pathway of birdsong. *Biol Cybern* 91: 159–167, 2004.

Akutagawa E and Konishi M. Connections of thalamic modulatory centers to the vocal control system of the zebra finch. *Proc Natl Acad Sci USA* 102: 14086–14091, 2005.

Appeltants D, Absil P, Balthazart J, and Ball GF. Identification of the origin of catecholaminergic inputs to HVc in canaries by retrograde tract tracing combined with tyrosine hydroxylase immunocytochemistry. *J Chem Neuroanat* 18: 117–133, 2000.

Bottjer SW, Miesner EA, and Arnold AP. Forebrain lesions disrupt development but not maintenance of song in passerine birds. *Science* 224: 901–903, 1984.

Cardin JA, Raksin JN, and Schmidt MF. Sensorimotor nucleus NIf is necessary for auditory processing but not vocal motor output in the avian song system. *J Neurophysiol* 93: 2157–2166, 2005.

Cardin JA and Schmidt MF. Song system auditory responses are stable and highly tuned during sedation, rapidly modulated and unselective during wakefulness, and suppressed by arousal. *J Neurophysiol* 90: 2884–2899, 2003.

Cardin JA and Schmidt MF. Auditory responses in multiple sensorimotor song system nuclei are co-modulated by behavioral state. *J Neurophysiol* 91: 2148–2163, 2004a.

Cardin JA and Schmidt MF. Noradrenergic inputs mediate state dependence of auditory responses in the avian song system. *J Neurosci* 24: 7745–7753, 2004b.

Chi Z and Margoliash D. Temporal precision and temporal drift in brain and behavior of zebra finch song. *Neuron* 32: 899–910, 2001.

Coleman MJ and Mooney R. Synaptic transformations underlying highly selective auditory representations of learned birdsong. *J Neurosci* 24: 7251–7265, 2004.

Dave AS and Margoliash D. Song replay during sleep and computational rules for sensorimotor vocal learning. *Science* 290: 812–816, 2000.

Dave AS, Yu AC, and Margoliash D. Behavioral state modulation of auditory activity in a vocal motor system. *Science* 282: 2250–2254, 1998.

Deregnaucourt S, Mitra PP, Fehér O, Pytte C, and Tchernichovski O. How sleep affects the developmental learning of bird song. *Nature* 433: 710–716, 2005.

Doupe AJ. A neural circuit specialized for vocal learning. *Curr Opin Neurobiol* 116: 104–111, 1993.

Doupe AJ, Solis MM, Kimpo R, and Boettiger CA. Cellular, circuit, and synaptic mechanisms in song learning. *Ann NY Acad Sci* 1016: 495–523, 2004.

Fee MS, Hahnloser HR, and Kozhevnikov AA. The origin of a representation of time in the brain. *2002 Abstract Viewer/Itinerary Planner*. Washington, DC: Society for Neuroscience, 2002, Online.

Fenn KM, Nusbaum HC, and Margoliash D. Consolidation during sleep of perceptual learning of spoken language. *Nature* 425: 614–616, 2003.

Fortune E and Margoliash D. Parallel pathways and convergence onto HVc and adjacent neostriatum of adult zebra finches (*Taeniopygia guttata*). *J Comp Neurol* 360: 413–441, 1995.

Foster EF and Bottjer SW. Lesions of a telencephalic nucleus in male zebra finches: influences on vocal behavior in juveniles and adults. *J Neurobiol* 46: 142–165, 2001.

Foster EF, Mehta RP, and Bottjer SW. Axonal connections of the medial magnocellular nucleus of the anterior neostriatum in zebra finches. *J Comp Neurol* 382: 364–381, 1997.

Gerstner W and Kistler W. *Spiking Neuron Models. Single Neurons, Populations, Plasticity*. Cambridge, UK: Cambridge Univ. Press, 2002.

Hahnloser R HR and Fee MS.. Single neuron recordings in nucleus interface of singing zebra finches. Program No. 294.4. *2003 Abstract Viewer/Itinerary Planner*. Washington, DC: Society for Neuroscience, 2003, Online.

Hahnloser RHR, Kozhevnikov AA, and Fee MS. An ultrasparse code underlies the generation of neural sequences in a songbird. *Nature* 419: 65–70, 2002.

Hahnloser RHR, Kozhevnikov AA, and Fee MS.Sleep-related neural activity in a premotor and a basal-ganglia pathway of the songbird. *J Neurophysiol* 96: 794–812, 2006.

Janata P and Margoliash D. Gradual emergence of song selectivity in sensorimotor structures of the male zebra finch song system. *J Neurosci* 19: 5108–5118, 1999.

Kao MH, Doupe AJ, and Brainard MS. Contributions of an avian basal ganglia-forebrain circuit to real-time modulation of song. *Nature* 433: 638–643, 2005.

Kimpo RR, Theunissen FE, and Doupe AJ. Propagation of correlated activity through multiple stages of a neural circuit. *J Neurosci* 23: 5750–5761, 2003.

Leonardo A and Fee MS. Ensemble coding of vocal control in birdsong. *J Neurosci* 19: 652–661, 2005.

Margoliash D. Do sleeping birds sing? Population coding and learning in the bird song system. *Prog Brain Res* 130: 319–331, 2001.

McCasland JS. Neuronal control of bird song production. *J Neurosci* 7: 23–39, 1987.

Mooney R. Different subthreshold mechanisms underlie song selectivity in identified HVc neurons of the zebra finch. *J Neurosci* 201: 5420–5436, 2000.

Nadasdy Z, Hirase H, Czurko A, Csicsvari J, and Buzsáki G. Replay and time compression of recurring spike sequences in the hippocampus. *J Neurosci* 19: 9497–9507, 1999.

Nottebohm F, Kelley DB, and Paton JA. Connections of vocal control nuclei in the canary telencephalon. *J Comp Neurol* 207: 344–357, 1982.

Okuhata S and Saito N. Synaptic connections of thalamo-cerebral vocal nuclei of the canary. *Brain Res Bull* 18: 35–44, 1987.

Olveczky BP, Andalman AS, and Fee MS. Vocal experimentation in the juvenile songbird requires a basal ganglia circuit. *PLoS Biol* 3: e153, 2005.

Palchykova S, Winsky-Sommerer R, Meerlo P, Dürr R, and Tobler I. Sleep deprivation impairs object recognition in mice. *Neurobiol Learn Mem* 85: 263–271, 2006.

Rosen MJ and Mooney R. Inhibitory and excitatory mechanisms underlying auditory responses to learned vocalizations in the songbird nucleus HVC. *Neuron* 39: 177–194, 2003.

Rosen MJ and Mooney R. Synaptic interactions underlying song-selectivity in the avian nucleus HVC revealed by dual intracellular recordings. *J Neurophysiol* 95: 1158–1175, 2006.

Scharff C and Nottebohm F. A comparative study of the behavioral deficits following lesions of various parts of the zebra finch song system: implications for vocal learning. *J Neurosci* 11: 2896–2913, 1991.

Shea SD and Margoliash D. Basal forebrain cholinergic modulation of auditory activity in the zebra finch song system. *Neuron* 40: 1213–1226, 2003.

Sohrabji F, Nordeen EJ, and Nordeen KW. Selective impairment of song learning following lesions of a forebrain nucleus in the juvenile zebra finch. *Behav Neural Biol* 53: 51–63, 1990.

Solis MM and Perkel DJ. Rhythmic activity in a forebrain vocal control nucleus in vitro. *J Neurosci* 25: 2811–2822, 2005.

Spiro JE, Dalva MB, and Mooney R. Long-range inhibition within the zebra finch song nucleus RA can coordinate the firing of multiple projection neurons. *J Neurophysiol* 81: 3007–3020, 1999.

Thomson DJ and Chave AD. (Editors). *Jackknifed Error Estimates for Spectra, Coherences, and Transfer Functions*. Englewood Cliffs, NJ: Prentice Hall, 1991.

Troyer TW and Doupe AJ. An associational model of birdsong sensorimotor learning. I. Efference copy and the learning of song syllables. *J Neurophysiol* 84: 1204–1223, 2000.

Vates GE, Broome BM, Mello CV, and Nottebohm F. Auditory pathways of caudal telencephalon and their relation to the song system of adult male zebra finches. *J Comp Neurol* 366: 613–642, 1996.

Walker MP and Stickgold R. Sleep, memory, and plasticity. *Annu Rev Psychol* 57: 139–166, 2006.

Yu AC and Margoliash D. Temporal hierarchical control of singing in birds. *Science* 273: 1871–1875, 1996.